

# chiral Quantum well Rashba splitting in Sb monolayer on Au(111)

Jinbang Hu<sup>1,\*</sup>, Lina Liu<sup>2</sup>, Xiansi Wang<sup>3</sup>, Yong P. Chen<sup>2</sup>, Justin W Wells<sup>1,4,\*</sup>

<sup>1</sup>*Department of Physics, NTNU, Trondheim, Norway.*

<sup>2</sup>*Institute of Physics and Astronomy and Villum Centers for Hybrid Quantum Materials and Devices, Aarhus University, 8000 Aarhus-C, Denmark.*

<sup>3</sup>*Hunan University, Changsha, 410082, China.*

<sup>4</sup>*Semiconductor Physics, Department of Physics, University of Oslo (UiO), NO-0371 Oslo, Norway.*

\*Corresponding author: jinbang.hu@ntnu.no; j.w.wells@fys.uio.no.

## Abstract

We present atomic and electronic structure investigations of Single-layer Sb(110) rhombohedral crystal formed on Au(111) substrate. Low energy electron diffraction (LEED) and scanning tunneling microscopy (STM) reveal a pure 2D Sb stripe structure, composed by a pair of Sb(110) unit cell located in a chiral configuration with mirror symmetry broken along the x axis direction. Based on angle-resolved photoemission spectroscopy (ARPES) measurement and Sb-weighted band structure from density functional theory calculations, we report the unambiguous determination of one pair of Rashba-type splitting band from the 2D Sb film, exhibiting a chiral symmetry in the electronic structure with the crossing point located at  $\bar{\Gamma}$  point and  $\bar{X}$  point, respectively. Moreover, From  $dI/dV$  spectra and calculated density of states(DOS), the quantum well(QW) Rashba-type states at different energy induced by the in-plane mirror symmetry broken in Sb stripe structure have been identified, and the orbital decomposition of projected band structure indicates hybridization between Sb  $p_y$  state and Au state can modify the spin splitting of QW states due to the intrinsic large SOC of Au state introduced into the QW states.

## INTRODUCTION

Manipulation of the spin degrees of the 2D gas confined in the ultrathin film plays an important role in the rapidly developing field of spintronics<sup>1-2</sup>. As the Rashba effect predicted by the theory, lifting of spin degeneracy originates from the spin-orbit coupling (SOC) in a inversion symmetry broken structures<sup>3</sup>. Especially for the structural inversion asymmetry induced by the surface-potential gradient from perpendicular to the substrate, a class of 2D surface alloys have been successfully fabricated on noble metal surface by substitution one out of three atoms within the topmost (111) surfaces forming a  $\sqrt{3} \times \sqrt{3}$  periodicity, for example, Pb, Bi, and Sb grown on Ag(111) and Cu(111), Sn on Au(111)<sup>4-10</sup> and the largest known Rashba spin splitting was reported for Ag<sub>2</sub>Bi, and also a number of prior studies of the 2D surface alloy have confirmed the important role played by the atomic SOC in determining the strength of the splitting. However, the electronic property of 2D adlayer, so far, has rarely been well discussed with in-plane asymmetry being considered. Similarly, like the Rashba splitting observed in 2D surface alloys, the ultra thin metal adlayer also exhibits spin-orbit splitting of the electronic states and, intriguingly, the asymmetric confinement from the interface potential can realize a further modification of electronic states, such as a giant spin-orbit splitting of QW states observed in the surface state of a Bi monolayer on Cu(111) due to the in-plane mirror symmetry broken in Bi adlayer<sup>11</sup>.

Apart from the easily preparation of a long-range ordered surface alloy superstructure, the single layer(SL) material may form several different reconstructions, and also the rotational of the domain determined by the symmetry of the substrate, leading to a extremely complicated 2D surface electronic structure. In the present work, based on STM observation of 2D Sb stripe structure formed on Au(111), we properly disentangle complicated surface electronic structure and studied the electronic structure originating from Sb(110) rhombohedral phase. Taking advantage of DFT calculation, the important role of symmetry broken played with the atomic orbital hybridization in determining the Rashba splitting with a chiral character has been confirmed, More further, a direct comparison between STS measurement and integrated the DOS around the  $\Gamma$  point helped to identified the Rashba splitting band as QW states located at different energy.

## EXPERIMENTAL AND THEORETICAL DETAILS

All sample preparation steps and experiments were performed under ultra-high vacuum conditions. The Au(111) surface was prepared by repeated sputtering and annealing cycles. The quality of the clean surface was confirmed by the STM observation of the well-known Au-herringbone reconstruction (Figure S1). Subsequently, Sb (purity 99.9999%) was deposited onto the clean surface at room temperature, yielding a 2D Sb(110) rhombohedral phase by subsequently annealing at 300 °C. During the evaporation, the pressure remained better than  $4 \times 10^{-10}$  mbar. The success of the sample preparation was confirmed by Low Energy Electron Diffraction (LEED). LT-STM/STS measurements carried out at 4 K were conducted using a Unisoku 1300 system. STS spectra were acquired using a commercial Pt-Ir tip with a standard lock-in technique with frequency of 917 Hz. Band structure measurements were performed at  $T \approx 115$  K using an aberration-corrected, energy-filtered photoemission electron microscope (EF-PEEM) (NanoESCA III, Scienta Omicron GmbH) equipped with a focused helium discharge lamp primarily generating He I photons at  $h\nu = 21.22$  eV, using pass energy  $E_p = 25$  eV and a 0.5 mm entrance slit to the energy filter, yielding nominal energy and momentum resolutions of  $\Delta E = 50$  meV and  $\Delta k = 0.02 \text{ \AA}^{-1}$ .

The density functional theory calculations were performed using the Vienna Ab initio Simulation Package (VASP)<sup>13</sup>. The interactions between the valence electrons and ion cores were described by the projector augmented wave method<sup>14</sup>. The electron exchange and correlation energy were treated by the generalized gradient approximation with the Perdew-Burke-Ernzerhof functional<sup>15-16</sup>. The kinetic energy cutoff of the plane-wave basis was set to 500 eV as default. For the matched models, The first Brillouin zone of SL Sb(110) on Au(111) system was sampled with the  $\bar{\Gamma}$ -centered  $6 \times 6 \times 1$  k points. The structures were optimized with symmetry (space group PM) until the forces on the atoms were less than  $10 \text{ meV \AA}^{-1}$ . The Au(111) surface was described by a periodic slab separated by 15 Å vacuum. 15 layers of Au atoms were included with the bottom 12 layers fixed as the bulk crystal structure while the top three layers were relaxed. One monolayer of Sb atoms was adsorbed on top side of the Au slab. In order to "unfold" the band structure with the symmetry of the primitive unit cell of SL Sb(110) and also the Au(111), we have calculated the effective band structure proposed by Popescu and Zunger<sup>17</sup> as implemented in the BandUp code<sup>18-19</sup>. The DOS is integrated over the zone center near the  $\bar{\Gamma}$  point with an momentum radius of  $k = 0.185 \text{ \AA}^{-1}$ . Spin-orbit coupling has been included for all band structure calculations. The STM image was simulated with a model of Sb  $3 \times \sqrt{3}$  superstructure on Au substrate with the Tersoff-Hamann approach<sup>20</sup>.

## RESULTS AND DISCUSSION

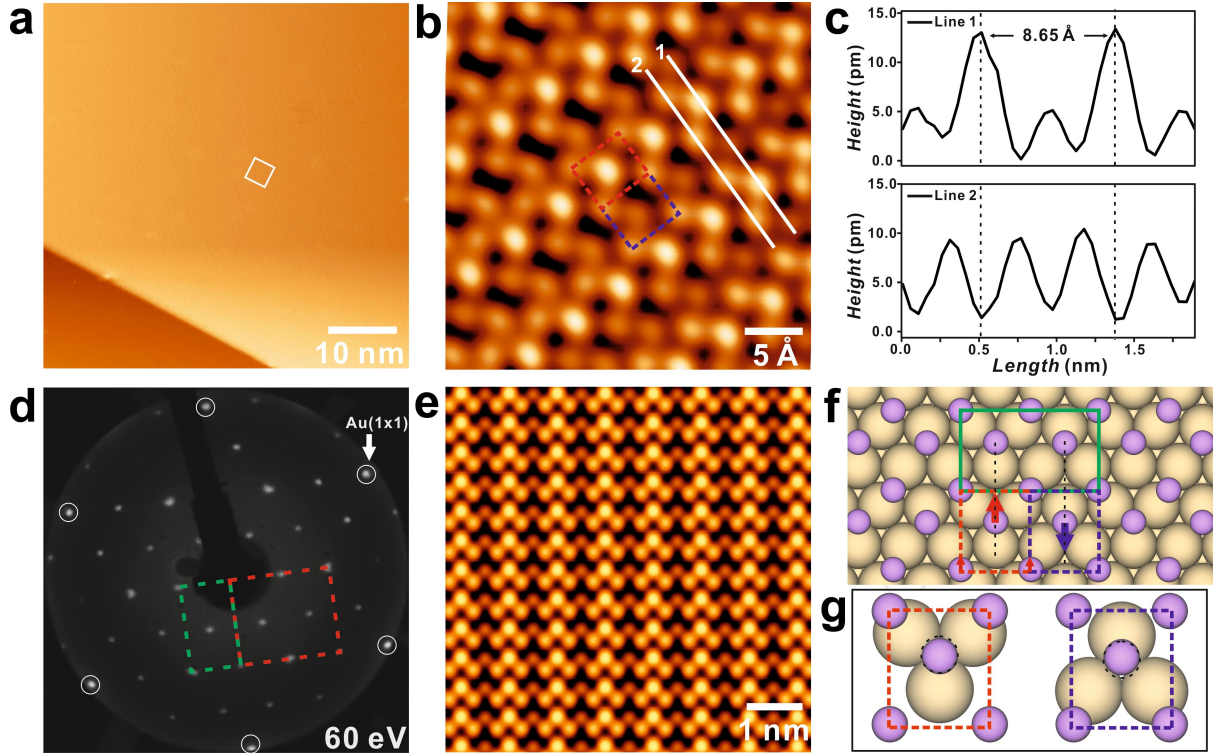


Figure 1. (a) Large scale STM image of monolayer Sb on the Au(111). (b) High-resolution STM image depicted by the white square in panel a, demonstrating a well-ordered  $3 \times \sqrt{3}$  reconstruction composed by the two adjacent Sb(110) unit cell marked by the blue and red dashed rectangular. (c) Line profile corresponding to the white line in panel b, revealing the periodicity 8.65 Å and mirror symmetry of the  $3 \times \sqrt{3}$  superstructure. (d) LEED pattern of 2D Sb film grown on the Au(111) taken at the beam energy of 60 eV. The corresponding reciprocal unit cell of  $3 \times \sqrt{3}$  reconstruction and the Sb(110) unit cell in (b) are indicated by the green and red dashed rectangular, respectively. (e) STM simulation of monolayer Sb on Au(111). (f) fully optimized slab lattice of the Sb  $3 \times \sqrt{3}$  superstructure, the blue and red arrow overlaid on two Sb atoms in two adjacent Sb(110) unit cell to explain the potential they experienced, and the mirror plane is marked by the black dashed line. (g) Schematic illustration of a pair of antiparallel potential generated by misalignment of the Sb atom in Sb(110) unit cell. The Sb located at threefold hollow sites of the substrate is marked by black dashed circle. Scanning parameters: (a) 1.4V, 0.78 nA; (b) 1.0V, 0.9 nA.

Figure 1 summarizes the monolayer structure of Sb on Au(111) fabricated by annealing of a thicker Sb film sample at 300 C°. The corresponding LEED pattern (Figure 1d) and STM image (Figure 1a,b) are much like what has been observed previously under a similar sample preparation conditions.<sup>12</sup> In Figure 1a, our STM observation reveals a typical large scale STM image of the sample, demonstrating a homogeneous stripe structure on the entire Au(111) surface. Figure 1b shows a zoomed-in STM image of the area designated by the white square in Figure 1a, revealing a well ordered  $3 \times \sqrt{3}$  reconstruction of the Sb stripe structure formed on Au(111). Moreover, the  $3 \times \sqrt{3}$  superstructure can be divided into two adjacent Sb(110) subunit cell, marked by the red and blue rectangular, differing obviously in the respective heights of the Sb atom in the middle. Correspondingly, the new spots appearing in the LEED pattern originate from the reciprocal unit cell of  $3 \times \sqrt{3}$  superstructure (green dashed rectangular) and Sb(110) subunit cell (red dashed rectangular) with three rotated symmetry.

In our study, we report rectangular supercell of the Sb stripe structure with a mirror symmetry. The line profile marked in Figure 1b differs the respective heights of the Sb atom in the Sb monolayer structure, as shown in Figure 1c, revealing the mirror symmetry in Sb  $3 \times \sqrt{3}$  superstructure and also in two Sb(110) subunit cell. The mirror plane for  $3 \times \sqrt{3}$  superstructure is along the brightest (or dimmest) line of Sb atom, which are also the mirror plane for two Sb(110) subunit cell, respectively. On the basis of the STM observation, the theoretically optimized structure of Sb on Au(111) is depicted in Figure 1f, and the corresponding STM simulated image (Figure 1e) well reproduced the

stripe feature with mirror symmetry in 2D Sb on Au(111). On closer inspection of the optimized structure, the commensurate rectangular  $3 \times \sqrt{3}$  stripe superstructure can also be expressed in its matrix form as  $\begin{pmatrix} 3 & 0 \\ 1 & 2 \end{pmatrix}$  referring to Au(111) surface or  $\begin{pmatrix} 2 & 0 \\ 0 & 1 \end{pmatrix}$  referring to Sb(110) rectangle unit cell. The Sb stripe superstructure can be divided into two Sb(110) sub-unit cells with the central Sb atom within the rectangle slightly misaligned to the threefold hollow sites of the Au substrate, as shown in Figure 1g. Hence, It can be expected that the Sb atom, marked by the arrow, in the centre of two adjacent Sb(110) unit cell experience an antiparallel potential gradient along the y direction since each Sb(110) unit cell represents a mirror symmetry along the y direction. The mirror plane is marked by the black dashed line in Figure 1f. In the perspective of the  $3 \times \sqrt{3}$  stripe superstructure, a pair of antiparallel potential generated by misalignment of the Sb atom in two adjacent Sb(110) unit cell can be invoked to illustrate the presence of chiral symmetry. The manifestation of chiral symmetry is also evident in the electronic properties, which will be expounded upon in the subsequent discussion.

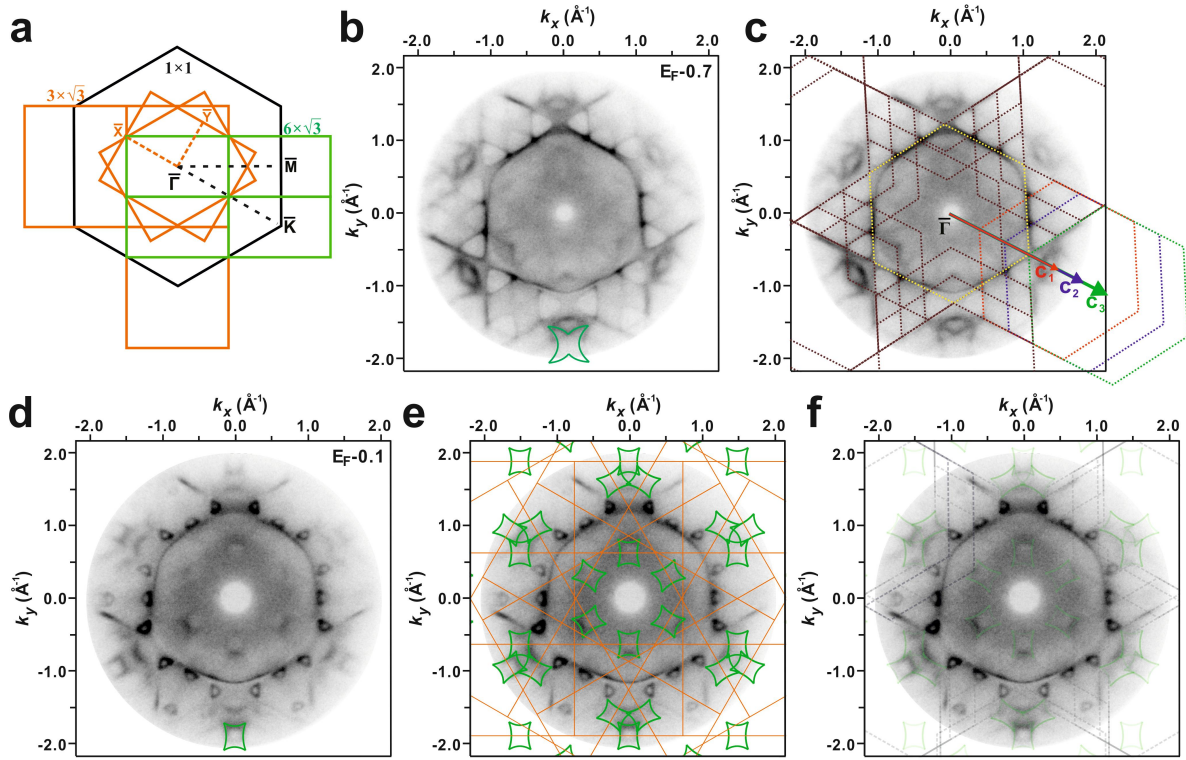


Figure 2. (a)  $1 \times 1$ , Sb(110) and  $3 \times \sqrt{3}$  surface Brillouin zone (SBZ) scheme for Au(111) surface, Sb(110) rhombohedral unit cell and Sb stripe superstructure, respectively. (b-f) constant energy contours from the Sb/Au(111)  $3 \times \sqrt{3}$  surface at 115K. The contours are shown at 0.7 eV (b,c) and 0.1 eV (d-f) below the Fermi level. The new appearing surface band feature marked as green flower. (c) dashed hexagon (in brown) drawn to trace the weak features appearing in the constant energy contours. The weak dashed hexagon originates from Umklapp scattering of Au sp band, marked by the bright dashed hexagon (in yellow). Three reciprocal lattice vectors marked as  $C_1$ ,  $C_2$  and  $C_3$  indicate the possible Umklapp scattering process. (e) Sb(110) SBZ with green-line marks appearing at  $\bar{X}$  point overlaid on the constant energy contours to trace the possible position of flower-shaped bands. (f) Umklapp scattering of Au sp band, combined with flower marks from the three different azimuthal orientations of the (110) rhombohedral phase fits on the constant energy contours.

We now turn to the electronic structure investigated by ARPES. Figure 2 shows the constant energy contours obtained from the Sb/Au(111)  $3 \times \sqrt{3}$  surface. In this section, we use constant energy contours at 0.7 eV below the Fermi level as an example to delve into a detailed electronic structure study of Umklapp scattering originating from Au sp band. Additionally, we employ a constant energy contour at 0.1 eV to elucidate the complex Umklapp scattering band induced by the three different azimuthal orientations of the Sb(110) rhombohedral lattice on the Au(111) surface. Figure 2a

presents the  $1 \times 1$  (black hexagon), Sb(110) (yellow rectangle) and  $3 \times \sqrt{3}$  (green rectangle) SBZ schemed for Au(111) surface, Sb(110) rhombohedral unit cell and Sb stripe superstructure, respectively. The three overlaid yellow rectangle indicates three rotational domains of Sb(110) rhombohedral unit cell, extending across the 1st Au(111) SBZ. As a comparison of Figure 2b and 2d, the weak triangle-shaped feature appearing at around the  $\bar{K}$  point of Au(111) SBZ shrink to smaller size with an increasing intensity of signal as the binding energy approaches the Fermi level. To understand the origin of the weak triangle features around the  $\bar{K}$  symmetry point, we have drawn brown dashed hexagons to trace the band features observed in the experimental constant energy contours. These brown dashed hexagons can be categorized into three groups, originating from three different Umklapp scattering processes of Au sp band (yellow dashed hexagon) with reciprocal lattice vectors marked as  $C_1$  (in red),  $C_2$  (in blue) and  $C_3$  (in green), respectively. A careful analysis reveals that  $C_1 = 4a_1 - a_2$ ,  $C_2 = 3a_2$ ,  $C_3 = 4a_1$ . Notice, we only use three types of Umklapp scattering vectors to set an example as well fitting of the weak triangle band features in experimental constant energy contours, there is highly possible of extra Umklapp scattering vectors being applied to tracing the triangle band feature in higher order SBZ of Au(111) surface, as well as the fuzzy background in the first Au(111) SBZ.

More further, the influence from three rotational domains of Sb(110) rhombohedral lattice has also been discussed to disentangle the flower-shaped band (marked by green line in Figure 2b and 2d), which can't be ascribed solely to the Umklapp scattering of Au sp band. Figure 2e represents the constant energy contour at the binding energy 0.1 eV overlaid by Sb(110) SBZ (orange rectangle) with the flower-shaped band located at  $\bar{X}$  point. The new schematic drawing of flower-shaped bands agree well with the experimental band features appearing at two side of  $\bar{M}$  points along  $\bar{\Gamma} - \bar{M}$  direction of Au(111) SBZ. Ultimately, Figure 2f confirms the veracity of the novel schematic rendering of the flower-shaped bands, harmoniously aligned with the encompassing larger hexagon-traced Umklapp pattern, thus eloquently corroborating the nature of the complicated surface bands feature engendered by the Sb/Au(111)  $3 \times \sqrt{3}$  surface. The well agreement of the Umklapp scattering band fitting with the complicated feature in ARPES data indicates the well-ordered Sb(110) rhombohedral structure formed in a 2D Sb film on Au(111).



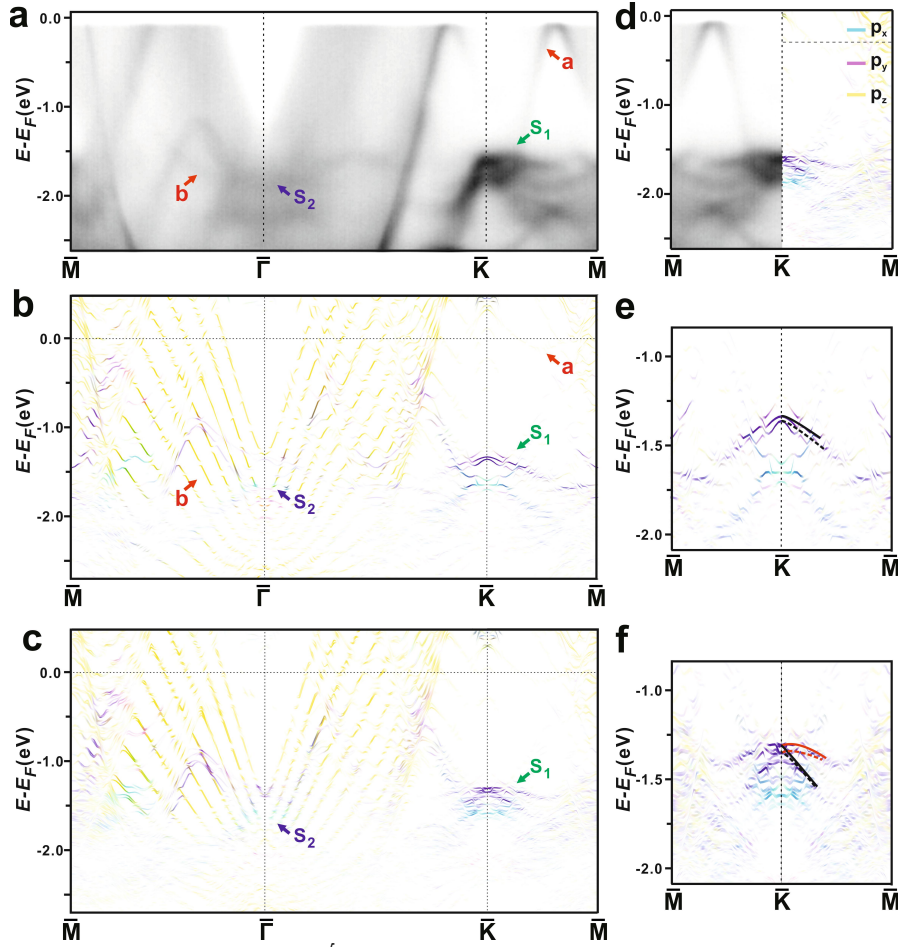


Figure 3. (a) ARPES results from the Sb/Au(111)  $3 \times \sqrt{3}$  surface along high-symmetry directions of the Au(111) SBZ. Dispersive features labelled b originate from three-dimensional bulk bands of Au(111). The labels  $S_1$  and  $S_2$  are used to denote the bands originating from the 2D Sb film. The label a originates from Umklapp scattering of Au sp band. Calculated band structure without SOC (b) and with SOC (c) for the optimized model of the Sb/Au(111) surface reconstruction shown in Figure 1e. Blue, pink and yellow symbols show contributions from  $p_x$ ,  $p_y$  and  $p_z$  states, respectively. (d) comparison between ARPES data and calculated band dispersion along  $\bar{K}-\bar{M}$  direction. The calculated bands shifted up by 0.3 eV to match the ARPES data. (e-f) comparison between calculated band dispersion along  $\bar{K}-\bar{M}$  direction without SOC (e) and with SOC (f) around  $\bar{K}$  point to illustrate the splitting of two pair of Rashba-type bands, marked by the dashed and solid line in red (spin up) and black (spin down) coded.

To gain further insight into the electronic structure of the 2D Sb film and to elucidate the origin of the Rashba-type spin-orbit splitting observed in our ARPES measurement, band structure calculations were performed based on a Sb  $3 \times \sqrt{3}$  superstructure possessing mirror symmetry of the two Sb(110) subunit cell as previously expounded. Figure 3b and 3c show such weighted band structure without SOC and with SOC projected from Sb monolayer, respectively. The calculated bands with SOC, as displayed in Figure 3c, exhibit a good overall agreement with the experimental bands in Figure 3a, apart from the band feature labelled as 'a' and 'b'. The feature a presents a discernibly akin band dispersion to that of the Au sp band, and its conspicuous absence within the calculated band structure correlates with our ascertained deduction of its origin emanating from Umklapp scattering of the Au sp band, which is in harmony with our discussion of the weak triangle-shaped feature observed in constant energy contours in Figure 2. Moreover, the new band features around the  $\bar{\Gamma}$  and  $\bar{K}$  point, labelled as  $S_1$  and  $S_2$  respectively, appearing in our ARPES measurement and calculated band structure projected from states of Sb indicates their contribution mainly originate from the topmost 2D Sb film. As show in Figure 3a, the several branches of  $S_1$  band feature show a strong photon emission intensity near the  $\bar{K}$  point and disperse downward away from a maximum energy at 1.55 eV below the Fermi level, while the band dispersion of feature  $S_2$  looks blurry, due to the overlapping with the replicas of the Au bulk band feature b, resulting from photo-excitation by the He I $\beta$  emission line of the nonmonochromatized He I light source.

In comparison with the weighted band structure without SOC in Figures 2b, one notices that the band feature  $S_1$  splits into two discernible parabolic sub-bands around the  $\bar{K}$  point after SOC is included, as shown in Figure 2c. Moreover, a directly comparison in Figure 3d shows a good agreement between DFT calculations and the experimental results along  $\bar{K} - \bar{M}$  direction, which confirms a typical feature of Rashba SOC presenting in the band feature  $S_1$ . Further analysis on the band structures projected on Sb p orbital (Figure 3c) indicates that the Rashba-type band feature  $S_1$  mainly consists of Sb  $p_y$  orbitals, and the band feature  $S_2$  donates from Sb  $p_x$  orbital. The  $p_z$  orbitals become indistinguishable and are strongly hybridized with Au substrate. In Figure 3e, f, the zoom-in band feature  $S_1$  along  $\bar{K} - \bar{M}$  direction shows two paralleled branch, marked by dashed and solid line, respectively, slightly gapped in energy around the  $\bar{K}$  points without SOC included, and with SOC, these two branch split into two pair of Rashba-type bands with separation in energy being further enhanced. We deduce the small energy discrepancy of the two pair of Rashba-type bands is caused by the Sb atom in the middle of two Sb(110) unit cell experiencing a different potential from Au substrate since the two Sb(110) unit cell in  $3 \times \sqrt{3}$  stripe structure buckling oppositely normal to Au(111) surface. Our further calculation of the Sb/Au(111)  $3 \times \sqrt{3}$  surface without buckling of the stripe superstructure confirmed the obviously decreasing separation of the two branch of  $S_1$  band(Figure S2).

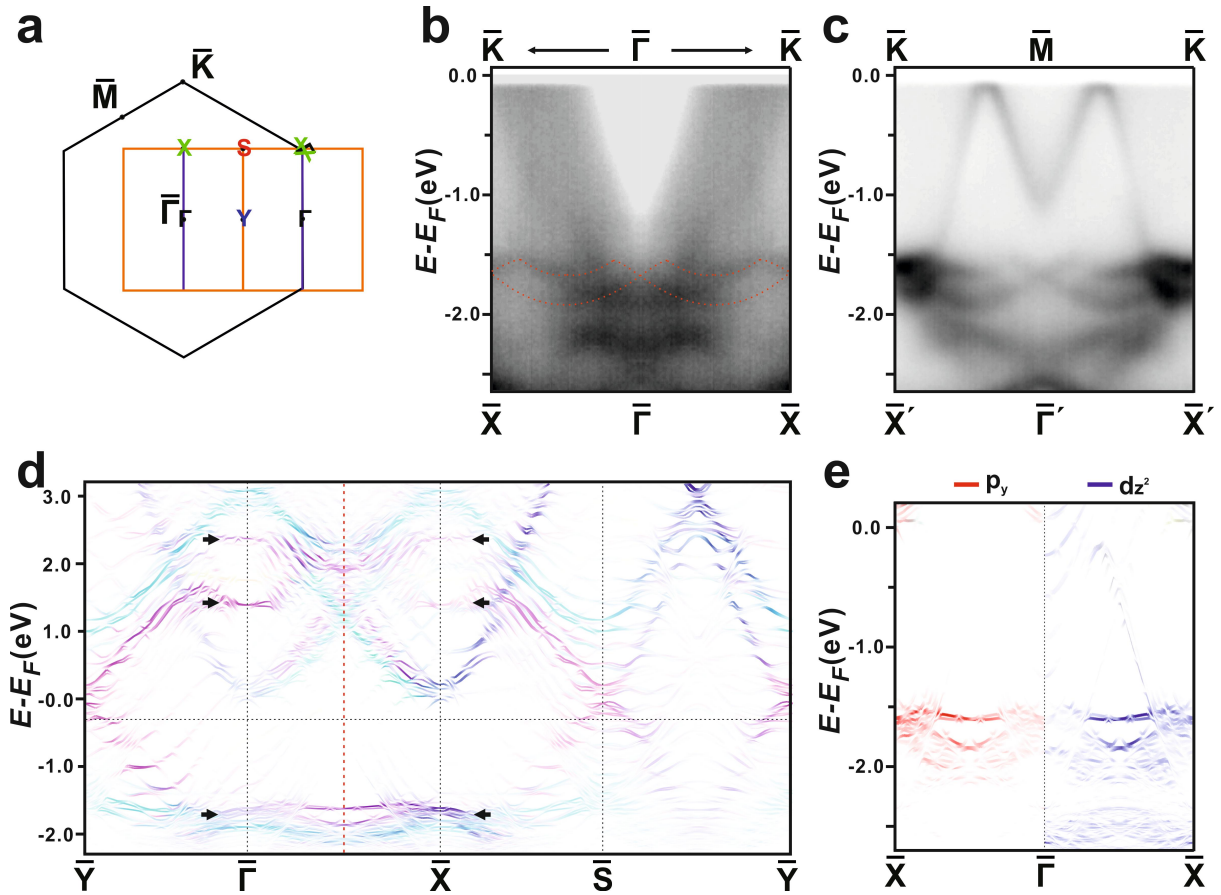


Figure 4. (a) the distribution of band feature from surface Sb(110) structure around Au(111) SBZ due to the three different azimuthal orientations of the Sb(110). The band structure around the high symmetry point of the Sb(110) sub-unit cell are symbolled by  $\Gamma$ , X, Y, and S respectively. (b-c) The ARPES results of Sb/Au(111)  $3 \times \sqrt{3}$  surface sliced along high-symmetry directions in the first Sb(110) SBZ (b) and the second SBZ (c) marked as blue line in (a), the red dashed pattern used to trace the Rashba splitting band discussed in Figure 3. (d). calculated band structure unfolded to SBZ of Sb(110) sub-unit cell exhibit a character of chiral symmetry. Light blue and pink symbols show contributions from  $p_x$  and  $p_y$  states of Sb topmost layer, respectively. The black arrow used to mark the energy position of QW states. The red dashed line used to mark the mirror plane. (e) calculated band structure projected from the  $d_{z^2}$  orbital (weighted by blue in the right side of the panel) of topmost Au layer and the  $p_y$  orbital (weighted by red in the left side of the panel) of topmost Sb surface layer to show a strong  $p_y$ - $d_{z^2}$  orbital hybrid character in the occupied QW state.

Figure 4a shows the distribution of band feature from surface Sb(110) structure extending over the Au(111) SBZ with band feature around the high symmetry point of the Sb(110) unit cell symbolled by  $\Gamma$ , X, Y, and S, respectively. Due to the three different azimuthal orientations of the Sb(110) rhombohedral lattice and the distinct in lattice parameters between Au(111) surface and Sb(110) unit cell, the band feature  $\Gamma$  and X meet at the  $\bar{K}$  point of Au(111) SBZ while the feature  $\Gamma$  from the 2nd SBZ of Sb(110) sub-unit cell appearing independently at the  $\bar{M}$  symmetry point of Au(111) SBZ. Figure 4b and 4c show the experimentally recorded band dispersion along  $\bar{\Gamma} - \bar{X}$  in the first Sb(110) SBZ (Figure 4b) and the second SBZ (Figure 4c) marked as blue line in Figure 4a, we found the Rashba-type splitting band  $S_1$  as we discussed above repeats to be periodic along  $\bar{\Gamma} - \bar{X}$  with respect to Sb(110) SBZ, since the symmetry path  $\bar{\Gamma} - \bar{X}$  of the second Sb(110) SBZ corresponds to the path  $\bar{M} - \bar{K}$  of Au(111) SBZ. This Rashba-type splitting band  $S_1$  shows a clear band feature along  $\bar{\Gamma} - \bar{X}$  in the 2nd SBZ of Sb(110)(or  $\bar{M} - \bar{K}$  of Au(111) SBZ), however, partially shielded by the Au bulk state in the 1st SBZ of Sb(110) and highlighted by the red dashed line in Figure 4b.

Interestingly, in Figure 4(c), it seems the feature of the Rashba-type splitting band connecting between  $\bar{\Gamma}$  and  $\bar{X}$  points shows a mirror symmetry with a mirrored plane positioned at the midpoint and perpendicular to the  $\bar{\Gamma} - \bar{X}$  Brillouin path. This mirror-symmetry Rashba-type splitting band shows a stronger intensity of the band crossing around the  $\bar{X}$  points than the crossing at  $\bar{\Gamma}$  points, due to the signal from the  $\bar{\Gamma}$  symmetry point meeting with the signal from the another two  $\bar{X}$  symmetry point in the 2nd Sb(110) SBZ (shown in Figure 4a). Carefully checking the energy of the crossing point at  $\bar{X}$  point and  $\bar{\Gamma}$  point in Figure 4c, it can be found that the binding energy of the Rashba splitting band at  $\bar{\Gamma}$  point is slightly higher than at  $\bar{X}$  points, which is in agreement with the energy separation of the two pair of Rashba-type band appearing at  $\bar{K}$  point of Au(111) SBZ, shown in Figure 3e-f.

As we claimed mirror symmetry in the Sb stripe superstructure perpendicular to x axis and the nice agreement between the DFT calculated band structure and ARPES data, we do a further analysis the role of a pair of antiparallel in-plane potential gradient along the y direction played on band structure. The absence of mirror symmetry perpendicular to the y-axis engenders a potential gradient along the y-direction. This gradient, in turn, serves as the driving force behind the possible emergence of QW states originating from the Sb  $p_y$  orbitals. Figure 4d shows the band structure unfolded to SBZ of Sb(110) sub-unit cell. Light blue and pink symbols show contributions from  $p_x$  and  $p_y$  states of Sb topmost layer, respectively. The three pair of QW states at different energy level, marked by the black arrow in Figure 4d, can be clearly observed at  $\bar{X}$  point and  $\bar{\Gamma}$  point, respectively. The projected  $p_x$  and  $p_y$  states along the  $\bar{Y} - \bar{\Gamma} - \bar{X} - \bar{Y}$  direction, overall, show a mirror symmetry with the mirror plane marked by the red dashed line in Figure 4d, which indicates the chiral properties of the three pair of QW states at  $\bar{X}$  point and  $\bar{\Gamma}$  point. Hence, the mirrored character of the occupied Rashba-type band  $S_1$  observed in our ARPES measurement and the calculated band structure projected from Sb topmost layer indicates the the chiral properties of the Rashba-type band  $S_1$ .

On contrary to the reported increasing spin splitting of QW states with the level of their binding energy in Bi(110) monolayer on Cu(111) system<sup>11</sup>, the QW states of Sb monolayer on Au(111) surface shows a inversely tendency of the Rashba spin splitting. Since Sb shows intrinsically weak SOC while SOC in Au is strong, the degree of the Rashba spin splitting in different level of QW states can be modified by hybridization with Au states. Besides the character of Sb  $p_y$  orbital appearing in the QW states, orbital decomposition of calculated band structure projected from the topmost Au layer indicates the contribution from the Au orbital. As we can see in Figure 4e, the occupied QW state at -1.60eV shows a strong hybrid character between Sb  $p_y$  orbital(weighted by red in the left side of the panel) and Au  $dz^2$  orbital(weighted by blue in the right side of the panel), the unoccupied QW state at 1.39eV shows a Sb  $p_y$ -Au  $p_x$  hybrid orbital character while the QW state at 2.37eV shows a weak hybrid character with Au states(Figure s4b,c). Even though the higher QW state shows the



tendency of increasing delocalization towards the vacuum due to the effective lowering of the vacuum barrier for the higher-lying states, we deduce the SOC plays a more important role in Rashba spin splitting degree.

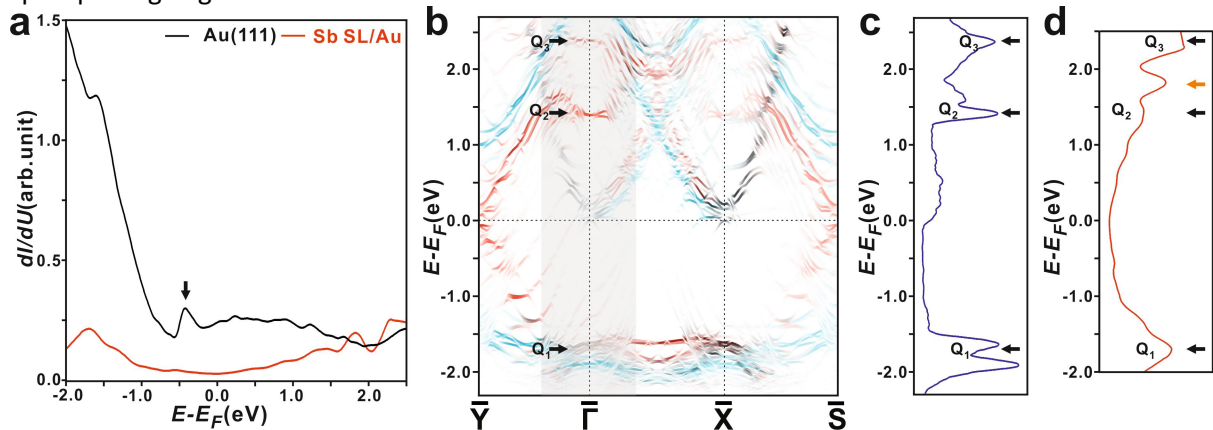


Figure 5. Electronic structures of QW states at different energy level. (a) Typical dI/dV spectrum obtained at centre regions of a large terrace of Sb stripe structure covered Au(111)(in red) and clean Au(111)(in black), acquisition conditions:  $U=+0.1$  V,  $I = 0.9$  nA,  $T = 4.0$  K,  $B=0$  T. (b) Orbital decomposed band structure of the 2D Sb  $3 \times \sqrt{3}$  surface covered Au(111). The blue and red indicate, respectively, the  $p_x$  and  $p_y$  orbital contributions. (c) The local (density of states)DOS integrated over the zone-center region near the  $\bar{\Gamma}$  point, marked by a gray shadow in (b), with a Gaussian broadening of 5.0 meV, in comparison with (d) our experimental dI/dV spectrum (in red) of the 2D Sb film. The crossings of the spin-orbit split occupied and unoccupied QW states at  $\bar{\Gamma}$  corresponding to the peak positions in (c) and (d) are marked with black arrows.

To determine the QW states at different energy positions induced by the absence of mirror symmetry perpendicular to the y-axis in Sb stripe structure, tunnelling spectra have been acquired in comparison with first-principle electronic structure calculations. Figure 5a displays the dI/dV spectrum taken in bias range from 2.5 to  $-2.0$  V on both Sb stripe structure covered Au(111)(in red) and clean Au(111)(in black). On Sb stripe structure covered Au(111), the Shockley surface state at  $-0.43$  V and an increasing background of density at high binding energy originating from clean Au(111) are obviously inhibited and several characteristic features appears, which indicates the corresponding electronic state mainly origin from the topmost Sb adlayer. Based on the Orbital decomposed band structure of the Sb stripe surface from the DFT calculations(Figure 5b),we further integrate the DOS around the  $\bar{\Gamma}$  point as shown in Figure 5c. Note that Our DFT calculations fairly support the peak corresponding to the QW states at different energy, marked by black arrow, observed in our STS measurement(Figure 5d), except an additional peak at around 1.8 eV, originating a hybrid state between Sb  $p_z$  orbital and Au  $dz^2$  orbital(Figure S5).

## SUMMARY

In our Letter, our STM observation confirmed SL Sb(110) rhombohedral crystal formed on Au(111). The Sb(110) unit cell possess mirror symmetry with a pair of antiparallel potential generated by misalignment of the Sb atom in two adjacent Sb(110) unit cell. we disentangle the intrinsic Sb(110) band from Umklapp scattered branches of Au sp band and the three different azimuthal orientations of the (110) rhombohedral phase. Further, we studied the role of the symmetry broken played on Sb(110) electronic structure. Our finding of three pair of QW Rashba splitting appearing at  $\bar{\Gamma}$  and  $\bar{X}$  symmetry point with a chiral character are fully confirmed by ARPES measurement , STS spectra and first-principles electronic structure calculations. We also explained the important role of strong spin-orbital coupling within the Au states played in hybridization with Sb  $p_y$  state to modify the spin splitting of QW states.

## ACKNOWLEDGMENT

This work was partially supported by the Research Council of Norway through its Centres of Excellence funding scheme, Project No. 262633, “QuSpin”. Lina Liu and Yong Chen acknowledge the support from Villim Investigator program (Grant No. 25931). X. S. W. acknowledges support from the

Natural Science Foundation of China (NSFC) Grant No. 12174093 and the Fundamental Research Funds for the Central Universities.

#### REFERENCE:

- 1 Anjan, S. et al. Emergent phenomena induced by spin–orbit coupling at surfaces and interfaces. *Nature* **539**, 509 (2016).
- 2 Manchon, A. et al. New perspectives for Rashba spin–orbit coupling. *Nat. Mater.* **14**, 871 (2015).
- 3 Rashba, E. et al. Properties of semiconductors with an extremum loop. 1. Cyclotron and combinational resonance in a magnetic field perpendicular to the plane of the loop. *Sov. Phys. Solid State* **2**, 1109 (1960).
- 4 Pacilé, D. et al. Electronic structure of an ordered Pb/Ag(111) surface alloy: Theory and experiment. *Physical Review B* **73**, 245429 (2006).
- 5 Moreschini, L. et al. Assessing the atomic contribution to the Rashba spin-orbit splitting in surface alloys: Sb/Ag(111). *Physical Review B* **79**, 075424 (2009).
- 6 Christian, R. et al. Giant Spin Splitting through Surface Alloying. *Physical Review Letters* **98**, 186807 (2007).
- 7 Maniraj, M. et al. Structure and electronic properties of the (3×3) R30° SnAu<sub>2</sub>/Au (111) surface alloy. *Physical Review B* **98**, 205419 (2018).
- 8 Shah, I. et al. Atomic and electronic structures of the Au<sub>2</sub>Sn surface alloy on Au(111). *Physical Review B* **104**, 125408 (2021).
- 9 Mirhosseini, H. et al. Unconventional spin topology in surface alloys with Rashba-type spin splitting. *Physical Review B* **79**, 245428 (2009).
- 10 Hendrik, B. et al. Spin orientation and sign of the Rashba splitting in Bi/Cu(111). *Physical Review B* **84**, 115426 (2011).
- 11 Mathias, S. et al. Quantum-Well-Induced Giant Spin-Orbit Splitting. *Physical Review Letters* **104**, 066802 (2010).
- 12 Cantero, E. D. et al. Synthesis and characterization of a pure 2d antimony film on au (111). *The Journal of Physical Chemistry C* **125**, 9273 (2021).
- 13 Kresse, G. & Joubert, D. From ultrasoft pseudopotentials to the projector augmented-wave method. *Physical Review B* **59**, 1758 (1999).
- 14 Blöchl, P. E. Projector augmented-wave method. *Physical Review B* **50**, 17953 (1994).
- 15 Perdew, J. P., Burke, K. & Ernzerhof, M. Generalized gradient approximation made simple. *Physical Review Letters* **77**, 3865 (1996).
- 16 Perdew, J. P., Burke, K. & Ernzerhof, M. Generalized Gradient Approximation Made Simple [Phys. Rev. Lett. 77, 3865 (1996)]. *Physical Review Letters* **78**, 1396 (1997).
- 17 Popescu, V. et al. Extracting E versus k effective band structure from supercell calculations on alloys and impurities. *Physical Review B* **85**, 085201 (2012).
- 18 Paulo, V. C. et al. Effects of extrinsic and intrinsic perturbations on the electronic structure of graphene: Retaining an effective primitive cell band structure by band unfolding. *Physical Review B* **89**, 041407 (2014).
- 19 Paulo, V. C. et al. Unfolding spinor wave functions and expectation values of general operators: Introducing the unfolding-density operator. *Physical Review B* **91**, 041116 (2015).
- 20 Tersoff, J.; Hamann, D. R. Theory of the scanning tunneling microscope. *Phys Rev B Condens Matter* **1985**, 31 (2), 805-813.

## Supporting information

### Chiral Quantum well Rashba splitting in Sb monolayer on Au(111)

Jinbang Hu<sup>1,\*</sup>, Lina Liu<sup>2</sup>, Xiansi Wang<sup>3</sup>, Yong P. Chen<sup>2</sup>, Justin W Wells<sup>1,4,\*</sup>

<sup>1</sup>*Department of Physics, NTNU, Trondheim, Norway.*

<sup>2</sup>*Institute of Physics and Astronomy and Villum Centers for Hybrid Quantum Materials and Devices, Aarhus University, 8000 Aarhus-C, Denmark.*

<sup>3</sup>*Hunan University, Changsha, 410082, China.*

<sup>4</sup>*Semiconductor Physics, Department of Physics, University of Oslo (UiO), NO-0371 Oslo, Norway.*

\*Corresponding author: jinbang.hu@ntnu.no; j.w.wells@fys.uio.no.

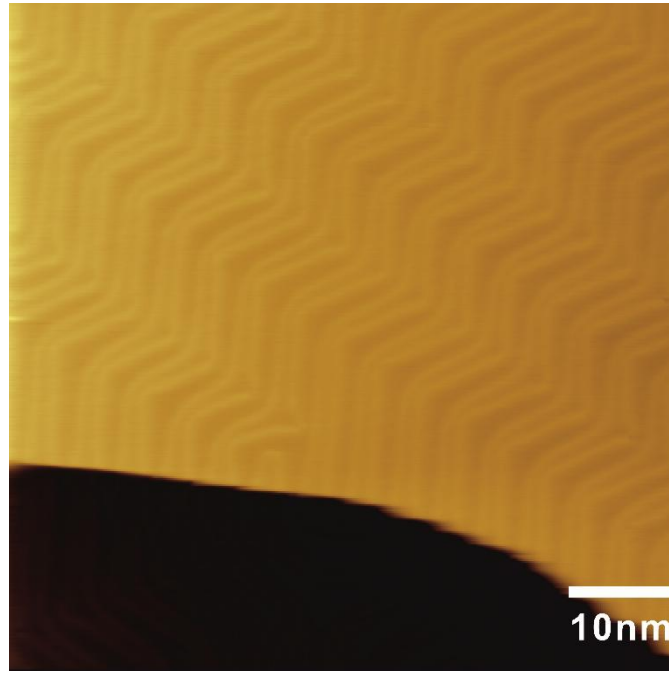


Figure S1. STM image of clean Au(111) surface before Sb deposition. Scanning parameters: -1.2V, 0.1 nA

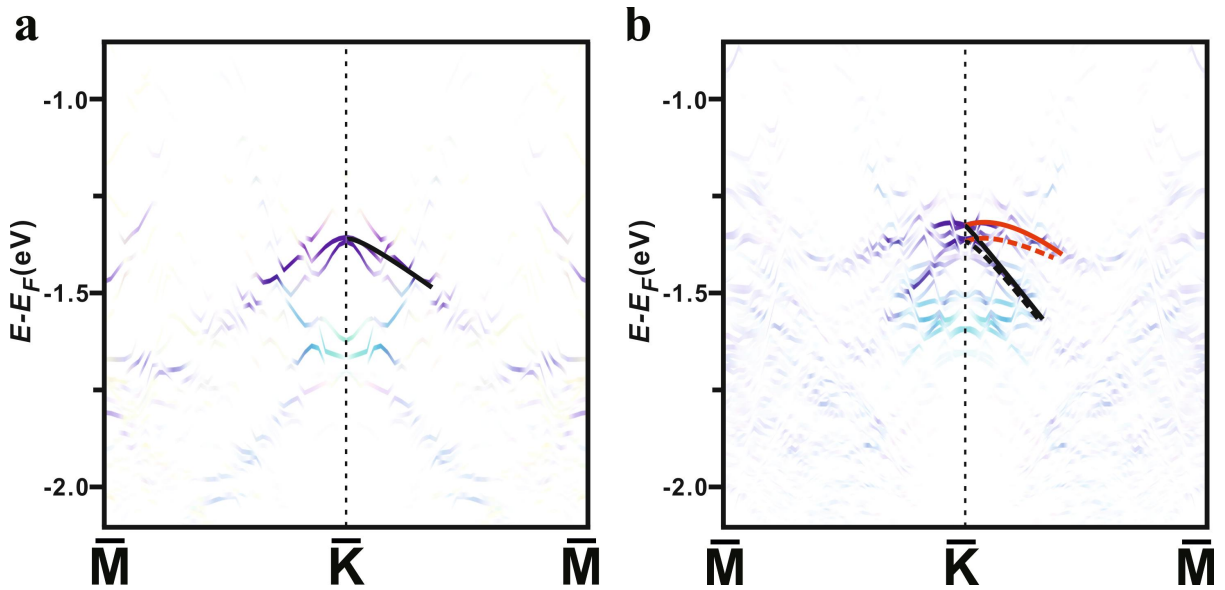


Figure S2. comparison between calculated band dispersion along  $\bar{K} - \bar{M}$  direction without SOC (a) and with SOC(b) around  $\bar{K}$  point to illustrate the splitting of two pair of Rashba-type band using a  $3 \times \sqrt{3}$  model of the Sb/Au(111) surface reconstruction without buckling of Sb topmost layer. yellow, blue, pink and purple symbols show contributions from  $p_z$ ,  $p_x$ ,  $p_y$  and  $p_x+p_y$  states, respectively.

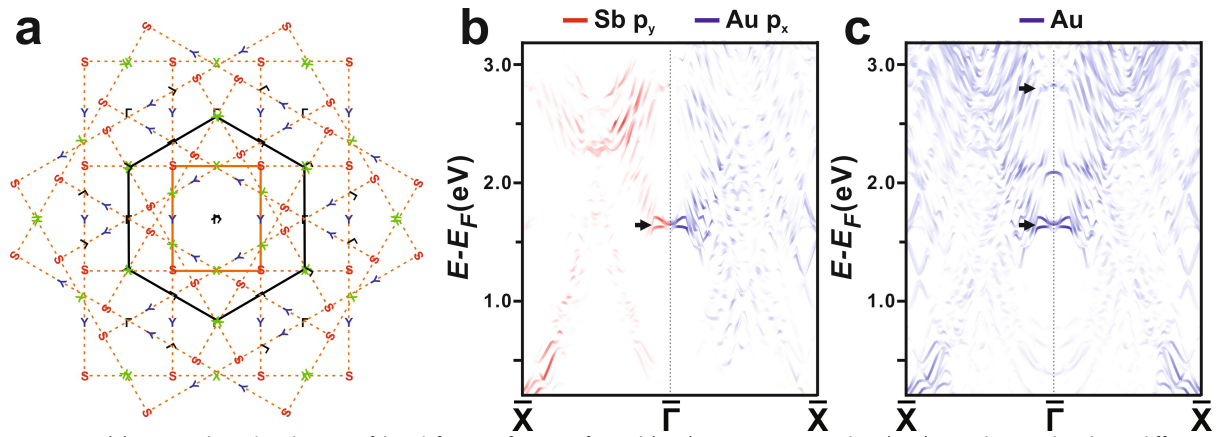


Figure S3. (a) A complete distribution of band feature from surface Sb(110) structure around Au(111) SBZ due to the three different azimuthal orientations of the Sb(110). The band structure around the high symmetry point of the Sb(110) sub-unit cell are symbolled by  $\Gamma$ ,  $X$ ,  $Y$ , and  $S$ , respectively. (b) calculated band structure projected from the  $p_x$  orbital (weighted by blue in the right side of the panel) of topmost Au layer and the  $p_y$  orbital (weighted by red in the left side of the panel) of topmost Sb surface layer to show a obvious  $p_x$ - $p_y$  orbital hybrid character in the occupied QW state, marked by the black arrow. (c) calculated band structure projected from the Au topmost layer to show a weak (strong) contribution from Au state to the QW state at 2.37 eV (1.36 eV), marked by the black arrow.

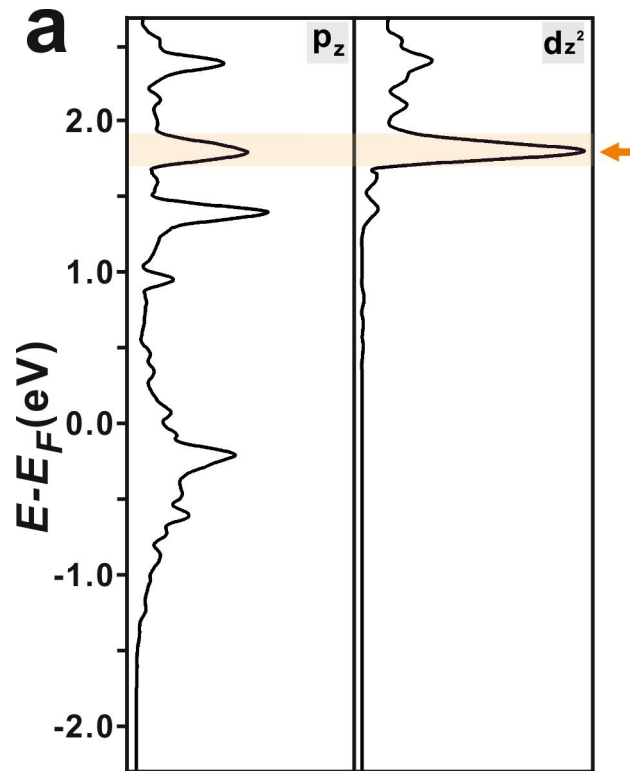


Figure S4. The Left (right) panel shows partial DOS integrated over the zone-center region near the  $\Gamma$  point of Sb  $p_z$  (Au  $d_{z^2}$ ) orbital-decomposed band structure from the Sb stripe surface (Au topmost layer).